Received: 29 September 2022 | Revised: 16 February 2023 | Accepted: 23 February 2023

DOI: 10.1002/appl.202200092

RESEARCH ARTICLE

Applied Research

Direct numerical simulation of the distribution of floating microplastic particles in an open channel flow

Yoshiyuki Sakai | **Michael Manhart**

Professorship of Hydromechanics, TUM School of Engineering and Design, Technical University of Munich, Munich, Germany

Correspondence
Yoshiyuki Sakai, TUM School of Engineering and Design, Technical University of Munich, Arcisstr. 21, 80333 Munich, Germany.
Email: yoshiyuki.sakai@tum.de

Funding information
Bundesministerium für Bildung und Forschung

Abstract

Microplastic fragments in the aquatic environment constitute a major threat for the health and fitness of organisms. However, our quantitative understanding in the microplastic load in typical natural river systems is severely limited due to the large uncertainties associated with the sources and the pathways of the microplastic contamination. To address this knowledge gap, we performed direct numerical simulations of the dynamics and distribution of microplastic particles in turbulent open channel flow at moderate Reynolds numbers. The particle dynamics is characterised by four nondimensional parameters, namely: Reynolds number of the open channel flow (Re_b), nondimensional particle diameter (d_p^+) and Galileo (Ga) and Stokes (St) numbers of the particles of which the latter two include the particle-fluid density ratio (β). To limit our scope to the most relevant configuration, we focused on the distribution of weakly buoyant microplastic particles at $\beta = 0.95$, whereas the remaining parameters were adjusted to cover the orders of magnitude that can be found in a typical laboratory facility, as well as a natural river. Our simulation results show that the steady-state microplastic distribution in the turbulent flow is influenced by the Stokes and the Galileo numbers significantly, which ranges from the complete accumulation on the free surface to the homogeneous distribution, and somewhere in between. Moreover, the Galileo number, alongside the flow Reynolds number, were also shown to influence the temporal scaling of the transient behaviour of the gradual accumulation of the microplastics towards the free surface. Both of our findings highlight the complex nature of the particle–turbulence interactions, and motivate further investigations in this approach.

KEYWORDS

direct numerical simulation, free surface turbulence, Maxey–Riley equation, microplastic, open channel flow

INTRODUCTION

Microplastic fragments in the aquatic environment constitute a major threat to aquatic organisms. There are various definitions of microplastics but historically plastic particles and fragments are denoted as microplastics when their size was below 5 mm [1]. The transport by surface waters constitutes one of the main sources of microplastic contamination in the ocean [2]. To identify sources and contamination pathways it necessary to estimate quantitatively the microplastic particle load effectuated by a river.

To evaluate quantitatively the net load by a river, several different sampling methods have been proposed [3–5]. Several sources of uncertainty, however, make it difficult to estimate the net load a river carries. Uncertainties in measurement method have been identified and discussed by, for example, Hildebrandt et al. [6]. Bannick et al. [7] have described uncertainties due to statistical scatter in a load of a river and proposed criteria for statistically representative sampling strategies in dependence of the particle load. Sample campaigns found large heterogeneity of microplastic concentrations among different sampling sites and across the river which might be caused by proximity of local sources, hydraulic conditions, mixing, and hydrological conditions [8].

The influence of local hydraulic conditions, mixing, and turbulence at the sampling site is one of the factors that introduce uncertainty into particle load. Taking local hydraulic conditions aside and assuming a flow in a straight river, we can assume an analogy between the natural river's flow and the turbulent flow in a laboratory flume. The dynamics of particles in a laboratory flume are functions of the particle density, diameter, carrier fluid's density, and viscosity, flow type/roughness, and Reynolds number. If the particles' size is smaller than the Kolmogorov length-scale, which is the theoretical smallest limit of the turbulent eddy size for a given condition, then a so-called point-particle approach can be used to approximate the dynamics of the particles (e.g., [9]).

In such an approach, the particles' velocity can be predicted at a good accuracy by the so-called Maxey–Riley equation in which spherical particle shapes are assumed [10]. This geometric simplification is well justifiable, especially in combination with the point particle approach in which the particle is assumed to be smaller than the smallest flow scales. Due to such scale differences, microscopic details of the particle shapes do not influence the hydrodynamic forces acting on the particles. In fact, spherical particles have been found to make a substantial share in microplastic particles found in rivers as reported, for example, by Mani et al. [8]. The Maxey–Riley equation takes into account several different effects. In many studies, only the Stokes drag between the carrier fluid and the particle has been considered, given that they consider the particles that are significantly heavier or lighter than the surrounding fluid (e.g., [11]). In the case of microplastic particles, with the small density difference between particle and carrier fluid, this assumption may lead to inaccurate results as small particles with a density close to the carrier fluid might follow the fluid nearly perfectly.

On the other hand, it is not possible to assume a homogeneous concentration of microplastic particles over the water column despite the small density difference. Some materials will have smaller and some will have larger densities than water and consequently, one can expect that lighter particles (smaller density) will float to the water surface in the long term whilst heavier particles (larger density) will eventually sink to the river or seabed. Observation in sediment transport have, however, shown that heavy sediment particles can have an equilibrium, or intermediate, distribution over the water column in the long-term sense—although they would sink down in a quiescent tank. The long-term distributions of sediment particles approximately follow the so-called Rouse profile which expresses the equilibrium between the turbulent mixing of particles over the vertical direction and the gravity acceleration towards the riverbed [12]. In this sense, the properties of the turbulent flow interact, or compete, with the particles' tendency to sink down to the bed or float up to the water surface. The vertical distribution of microplastic particles in a surface water is therefore not only dependent on the particle properties, but also the flow conditions of the carrier fluid (water).

However, most of the previous studies mentioned so far focused on the particles that are slightly or significantly heavier than the carrying fluid, since their primary objectives are often to study sediment dynamics. Due to this trend, the interaction between particles and the free surface with the underlying turbulence has not been studied in detailed. It is therefore important to establish our understanding of the particle–turbulence interactions with lighter particles in the environment where the free surface also interacts with turbulent flow.

Consequently, the objective of the current contribution is to simulate and study the dynamics of the microplastic particles that are transported in turbulent stream through a natural river or an experimental flume. In this study, we exclusively consider the microplastic particles that are slightly lighter than water that tend to float on the free surface. Our main focus is on the long-term particle concentration profile depending on the particle parameters, which are tailored to a range of values that is typical to microplastic particles, as well as the flow condition. Those parameters represent a balance between the turbulence mixing in the vertical direction and the gravitational acceleration trying to accumulate the microplastic particles on the free surface. Moreover, we study the temporal evolution of the particle concentration, which answers our question of how long it takes for the steady-state concentration profiles to emerge, and which of the flow and the particle parameters influence the evolution time. Overall we aim to address the uncertainties that are inherent in the microplastic samplings, either in natural rivers or laboratory setups. We simulate the fluid flow by means of direct numerical simulation, whilst the particle dynamics are represented by the point-particle approach by solving the Maxey–Riley equation.

NUMERICAL METHODS

Our numerical simulation approach consists of two coupled modules: the flow simulation and the particle simulation. The flow simulation is performed based on a conventional finite-volume method on a

stationary grid, whereas the dynamics of the particles are represented by a Lagrangian method. Therefore, the overall procedure is an Euler–Lagrange method for the simulation of particles in a turbulent flow. Such methods are often used for particle-laden flows with small volume fractions, to predict the precise dynamics of the particles.

Flow solver

We employ the direct numerical simulation (DNS) technique which solves the governing equations of fluid motions, namely incompressible Navier–Stokes equations with spatiotemporal resolutions which are high enough to resolve all the relevant scales. Hence no uncertainties from empirical turbulence models are involved. In this project, our in-house flow solver called MGLET [13, 14] was employed.

MGLET is capable of performing DNS and large-Eddy simulations (LES) of turbulent flows in arbitrary-shaped domains, which can be optionally coupled with transport of multiple scalar quantities as well as point particles. The code employs a finite-volume method to solve the following incompressible Navier–Stokes equations for the primitive variables (i.e., velocity and pressure).

$$\nabla \cdot \vec{u} = 0, \tag{1}$$

$$\frac{\partial \vec{u}}{\partial t} + (\vec{u} \cdot \nabla)\vec{u} = -\frac{1}{\rho_f}\nabla p + \nu \nabla^2 \vec{u}, \tag{2}$$

where $\vec{u}$ is fluid velocity vector, p is pressure and ρ_f and ν are kinematic viscosity and density of the fluid, respectively.

Those variables are stored in a Cartesian grid with staggered arrangement and discretised in space by a second-order central scheme. The time integration is done by an explicit third-order low-storage Runge–Kutta scheme [15]. The pressure computation is decoupled from the velocity computation by Chorin's projection method [16], which means a Poisson equation is to be solved for the pressure for each Runge–Kutta substep. Arbitrarily curved and geometrically complex surfaces are handled by a mass-conserving immersed boundary method [14, 17, 18]. A conventional domain decomposition is adopted for parallelisation, which is combined with a local grid refinement strategy. The local refinement is achieved by adding grid boxes with finer resolutions in an octree-like, hierarchical and overlapping manner, where the degree of grid refinement is determined by the grid levels [13].

The code is written in Fortran, and the communication between different processes is implemented via message passing interface (MPI), whereas an efficient parallel I/O strategy is implemented based on HDF5. The code exhibits a satisfactory strong scaling up to a problem size of ≈17 billion discrete cells distributed over approximately 32,000 parallel processes (cf. [19]), whilst a sufficient weak scaling was demonstrated up to 135,000 parallel processes.

Particle solver

We employ so-called "one-way" coupled point particle simulation of spherical microplastic particles in a turbulent flow. The term "one-way" implies that the particles are transported by the flow but do not have any feedback effect on the flow. These simplifications are possible if the particle diameters d_p are small compared to the smallest length-scale of the flow field and the volume fraction of the particles (ϕ_p) remains small so that the flow is not influenced by the particles. The commonly accepted upper limit of ϕ_p for the one-way coupling approach is $O(10^{-6})$ [20]. Similarly, the term "point" particles means that the spatial extent of the particles with respect to the numerical grid is so small that they can be treated as a point. Consequently, the particles and their flow around them are not spatially resolved. Instead, the global momentum balance for a particle is modelled from several force components, which are formulated in the so-called Maxey–Riley equation. Those forces are used to solve Newton's equation of motion for discrete point particles and thus simulate their motion in the fluid phase.

The Maxey–Riley equation describes the acceleration of a particle suspended in a fluid (left-hand side) based on the balance of the forces that the particle is subjected to (right-hand side)

$$\begin{aligned}\frac{du_{p,i}}{dt} = &\underbrace{\frac{\rho_p - \rho_f}{\rho_p} g_i}_{\text{buoyancy}} + \underbrace{\frac{\rho_f}{\rho_p}\left(\frac{\partial u_i}{\partial t} + u_{@p,j}\frac{\partial u_i}{\partial x_j}\right)}_{\text{fluid acceleration}} + \underbrace{\frac{1}{\tau_p}\left(u_{@p,i} - u_{p,i} + \frac{d_p^2}{24}\frac{\partial^2 u_i}{\partial x_j^2}\right)}_{\text{Stokes drag}} \\ &+ \underbrace{\frac{\rho_f}{2\rho_p}\frac{d}{dt}\left(u_{@p,i} - u_{p,i} + \frac{d_p^2}{40}\frac{\partial^2 u_i}{\partial x_j^2}\right)}_{\text{added mass}} \\ &+ \underbrace{\frac{d_p}{2\tau_p}\int_0^t \frac{\frac{d}{dt}\left(u_{@p,i} - u_{p,i} + \frac{d_p^2}{24}\frac{\partial^2 u_i}{\partial x_j^2}\right)}{\sqrt{\pi\nu(t-\tau)}} d\tau}_{\text{Basset history}},\end{aligned} \tag{3}$$

where $u_{p,i}$ is ith component of particle velocity vector, ρ_p is particle density, g_i is gravitational acceleration that is nonzero only in the wall-normal direction, and $u_{@p,j}$ is the fluid velocity at the particle location. Finally, $\tau_p = \frac{\beta d_p^2}{18\nu}$ is the particle time-scale.

The first term is the so-called *buoyancy force* term and as the name suggests, the force due to buoyancy generated by the density differences of particle and fluid. The second term—the *fluid acceleration* term—models the force on the particle that would occur if the particle were replaced by a fluid control volume.

The third term is called *Stokes drag force* term and describes the drag force experienced by the particle when it moves at a different velocity than the surrounding fluid. It contains the so-called Faxén correction, which takes into account the finite-size effect of the particle in the limit of low particle Reynolds number (Re_p). The finite particle Reynolds number effect can be incorporated by replacing the above Stokes drag term by:

$$\frac{C_D Re_p}{24\tau_p}\left(u_{@p,i} - u_{p,i} + \frac{d_p^2}{24}\frac{\partial^2 u_i}{\partial x_j^2}\right) \tag{4}$$

where the drag coefficient C_D depends on Re_p. This Reynolds number dependency stems from the flow separation and recirculation, and the vortex shedding behind the particle.

Based on an extensive literature review, Clift et al. [21] recommended a piecewise function C_D. Accordingly, our implementation follows:

$$C_D(Re_p) = \begin{cases} \frac{3}{16} + \frac{24}{Re_p}, & \text{if } Re_p < 0.01, \\ \frac{24}{Re_p}(1 + 0.15Re_p^{0.687}) + \frac{0.42}{1 + 4.25 \times 10^4/Re_p^{1.16}}, & \text{if } 0.01 < Re_p < 3 \times 10^5, \\ 29.78 + 5.3\log_{10} Re_p, & \text{if } 3 \times 10^5 < Re_p < 4 \times 10^5, \\ 0.1\log_{10} Re_p - 0.49, & \text{if } 4 \times 10^5 < Re_p < 10^6, \\ 0.19 - \frac{8 \times 10^8}{Re_p}, & \text{if } Re_p > 10^6. \end{cases} \tag{5}$$

Note that in the limit of very small Re_p, the original Stokes drag formulation in Equation (3) is restored.

The fourth term in Equation (3) describes the inertial forces of the surrounding fluid when the particle is accelerated and is called the *added-mass* term. It results in a delayed relaxation of the particle in the direction of the velocity of the surrounding fluid.

The last (fifth) term describes the temporal development of the boundary layer surrounding the particle (e.g., thickening) and therefore results in a memory term. This so-called *Basset history* term is often ignored in the studies considering heavy particles, however, there is an increasing number of recent studies demonstrating that it has a significant influence when the particle is close to neutrally buoyant [22–27]. Incorporating this history term is very costly not only in terms of computation but also the memory requirement due to the very slowly decaying kernel, therefore we opted for the efficient second-order method of van Hinsberg et al. [26]. This method integrates the convolution function over a finite widow, whilst approximating the rest by exponential functions. In the current study, we set the width of the integration window N to be at 32, whereas the number of the exponential functions m is at 10.

All of the above forces are expected to play nonnegligible roles in the dynamics of (nearly) neutrally buoyant particles being suspended in turbulent flow [9], therefore our simulations include them all.

The Maxey–Riley equation describes the particle acceleration as a function of the fluid velocity at the particle position $\vec{u}_{@p}$ and the particle velocity $\vec{u}_p$. Since the particles are usually not located at the points that define the numerical grid, the fluid velocity must be interpolated to the respective particle positions. Among many other alternative approaches, in MGLET a conservative second-order method has been implemented [28]. For each individual particle, the time integration of the Maxey–Riley equation gives the instantaneous velocity. To circumvent the stiffness of this equation, a so-called Rosenbrock–Wanner method is adopted, which treats the linear and nonlinear terms separately via implicit and explicit fourth-order Runge-Kutta integration schemes. Finally, the particle positions are determined with the help of an explicit integration of the velocities.

CONFIGURATIONS AND PARAMETERS

Governing parameters

We simulate a fully developed turbulent flow through an open channel with a perfectly smooth no-slip bottom wall and no side walls (see Figure 1). The streamwise extent and the width of the channel are infinite, which are realised by the periodic boundary condition being applied in the streamwise and the spanwise directions. The flow is characterised by a dimensionless number called the Reynolds number, which consists of the flow depth h (m), the fluid kinematic viscosity ν (m^2/s), as well as a representative velocity scale. In the literature, two variants of the Reynolds number are frequently used, namely the friction Reynolds number:

$$Re_\tau = \frac{u_\tau h}{\nu}, \tag{6}$$

and the bulk Reynolds number:

$$Re_b = \frac{u_b h}{\nu}, \tag{7}$$

where u_τ and u_b are the friction and the depth-averaged (or bulk) velocities respectively. The friction velocity is defined as $u_\tau = (\tau_w/\rho_f)^{0.5}$, where τ_w is the average wall shear stress and ρ_f is the fluid density as before. Note that both Reynolds numbers are related through the skin-friction coefficient c_f, therefore setting one determines the other.

Another governing dimensionless number which is relevant in the context of the natural river flow is the Froude number (Fr), which is the ratio of the inertia to the gravitational forces. In the current

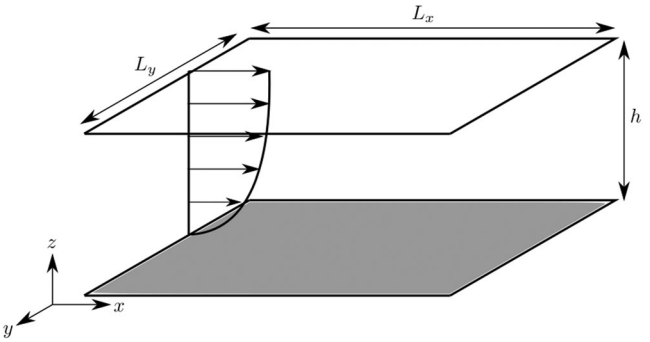

FIGURE 1 Schematic of the simulation domain.

study, we assume this dimensional number is so small that the free surface can be simply represented by an impermeable free-slip boundary. Note that this simplification approach has been adopted in a majority of the previous open channel simulation studies (e.g., [29–36]). Physically, this zero Froude number limit means any disturbance in the free surface is immediately flattened by gravity. These simplifications imply that in the idealised situation, the natural river flow can be characterised by the Reynolds number alone. This governing dimensionless parameter is though usually much higher in the natural river flow than what any DNS simulation code can achieve as of today.

On the other hand, the dynamics of small particles in turbulent flow can be characterised by the following parameters: the particle diameter d_p (m), the particle-fluid density ratio $\beta = \rho_p/\rho_f$, and the gravitational acceleration g (m/s^2) that contributes to up- or downward particle motions due to buoyancy. Consequently, three particle-related dimensionless numbers can be defined describing the dynamics of particles, namely a dimensionless particle diameter:

$$d_p^+ = \frac{d_p u_\tau}{\nu}, \tag{8}$$

the Stokes number:

$$St = \frac{\beta}{18}\left(\frac{d_p u_\tau}{\nu}\right)^2 = \frac{\beta}{18}(d_p^+)^2, \tag{9}$$

and the Galileo number:

$$Ga = \frac{\sqrt{|1-\beta|gd_p^3}}{\nu} = \frac{u_g d_p}{\nu}, \tag{10}$$

where $u_g = \sqrt{|1-\beta|gd_p}$. In this set of dimensionless parameters, β does not explicitly appear but is implicitly contained in St and Ga.

The dimensionless particle diameter quantifies the ratio of the particle diameter to a representative size of turbulent vortices. The Stokes number is often interpreted as the ratio of time-scales between particle and fluid. When St is large, the inertia of the particles cannot be neglected, and lead to ballistic motion—implying that the trajectories are barely influenced by underlying fluid velocity variations. The Galileo number describes the ratio of the gravitational to the viscous forces experienced by particles. This nondimensional number can also be interpreted as a particle Reynolds number based on the gravitational velocity-scale u_g.

Another relevant velocity scale is the terminal particle rising/sinking velocity due to buoyancy in a quiescent viscous fluid, $u_t = |1-\beta|gd_p^2/\nu$. Correspondingly, we can express Ga in terms of u_t as:

$$Ga = \sqrt{\frac{u_t d_p}{\nu}}. \tag{11}$$

Orders of magnitude of the parameters in natural flow

In the previous section, we showed that the dynamics of microplastics in turbulent open channel flow can be described in terms of the following dimensionless numbers, namely Re_τ, d_p^+, St and Ga. In the following, we estimate the orders of magnitude for those governing parameters in a real-world flow.

The Reynolds number of natural rivers based on bulk velocity can vary greatly, however, $Re_b = O(10^6)$ can be taken as a reasonable order of magnitude. This estimation is based on the water depth of $h = 1$ (m), the bulk velocity of $u_b = 1$ (ms^{-1}) and the kinematic viscosity of water $\nu = 10^{-6}$ (m^2/s). On the other hand, a typical experimental flume can be operated at $Re_b \sim O(10^5)$ with depth $h = 0.5-1$ (m), and the bulk velocity $u_b = 0.1$ (ms^{-1}). These Re_b can be converted to the corresponding Re_τ by an empirical relation, such as von Prandtl–Colebrook formula, which gives us the estimated order of magnitudes of $Re_\tau \sim O(10^4)$ for the natural river flow, and $Re_\tau \sim O(10^3)$ for the laboratory flume. Note that whilst the Reynolds number range for the natural river is beyond the reach of the DNS approach even using the world-fastest supercomputers, the laboratory flume range is somewhat achievable with a great expense of modern computing power, albeit it is beyond the scope of the current study. Nevertheless, these numbers will be used to determine the subsequent parameters for microplastic particles.

From the fluid dynamics viewpoint, the key challenge in our study is to cope with the broad range of density and size distributions of microplastics. Typically the size of microplastics decreases with time through mechanical, biological or chemical degradation processes, but it can also increase by biofilm growing on their surface. Furthermore, this growth of biofilm, which mainly consists of water, transforms microplastics to more neutrally buoyant properties. If some fouling organisms are attached to microplastics, however, their density can even be heavier than water leading to sinking [37, 38]. Seasonal variation of water temperature in rivers and oceans throws an additional complexity to the problem, since the density of the surrounding fluid will react to the temperature change whilst the solid density usually does not. Therefore a microplastic particle shows very different dynamical characteristics throughout its life, depending on the conditions of the surrounding flow and at which stage of the ageing process it is. This necessitates a wide area of parameter space to be explored to understand the dynamics of the microplastics in nature.

In this study, we consider $10 \lesssim d_p \lesssim 100$ (μm) as the representative diameter range of the microplastic particles in a natural river. Alternatively, the same particles represent $100 \lesssim d_p \lesssim 1000$ (μm) in the flow condition in an experimental flume. When we nondimensionalise these d_p values using $Re_\tau = 32{,}000$ (natural river), then d_p^+ ranges between 0.32 and 3.2. Conversely, if we assume $Re_\tau = 4200$ (exp. flume), then the corresponding d_p^+ ranges between 0.8 and 8.4. Furthermore, we consider a value of β, namely at 0.95 (slightly lighter than water), which approximately corresponds to polyethylene (PE) and polystyrene (PS). They are two of the most commonly identified plastic types in the marine environment [39].

Consequently, the upper limits of the number of microplastics per 1 (m^3) of water are respectively: $O(10^9)$ for $d_p = 10$ (μm) and $O(10^6)$ for $d_p = 100$ (μm), to fulfil the requirement for the one-way

TABLE 1 Flow simulation parameters.

Re_τ	Δx^+	Δy^+	Δz^+_{min}	Δz^+_{max}	$N_x \times N_y \times N_z$	$\Delta T u_\tau^2/\nu$	$\Delta T u_b/h$
180	8.44	4.22	0.9	3.3	256 × 256 × 96	15310	1329
400	4.8	2.4	0.34	2.72	990 × 990 × 256	12600	549

coupling approach ($\phi_p < 10^{-6}$). The actual number of microplastic particles found in the natural water is well below these thresholds [40].

Simulation parameters

In all simulations performed for this study, we first run the flow simulation until a developed statistically steady-state has been achieved before the microplastic particles were released. In this project, we simulated relatively low Reynolds numbers at Re_τ = 180 and 400. In both cases, the simulation domain covers $[L_x/h, L_y/h, L_z/h] = [12, 6, 1]$, where the subscripts x, y, z correspond to the streamwise, the spanwise and the flow-depth direction, respectively, whilst h is the channel full height as before. The grid resolutions were determined based on the reference in the literature and own experiences with the same code and flow [41, 42], and are summarised in Table 1.

In all cases, a constant timestep size Δt was adopted, and the sufficiency of the temporal resolution was ensured by keeping the maximum CFL number below 0.5. This also implies uniform window sizes for the Basset history term computation, which are at $5.45\nu/u_\tau^2$ and $7.35 \times 10^{-1}\nu/u_\tau^2$ for Re_τ = 180 and 400, respectively. The averaging time to achieve the statistically steady-state (ΔT) of the turbulent velocity statistics can also be found in Table 1.

As mentioned, the density ratio β was fixed at 0.95. The particle diameters and g were selected based on the ranges of the Stokes number and the Galileo number that were identified in the natural rivers and the laboratory flumes, namely $5 \times 10^{-2} \precsim St \precsim 5 \times 10^{0}$ and $0.3 \precsim Ga \precsim 7.1$ ($10^{-1} \precsim Ga^2 \precsim 5 \times 10^{1}$). We distributed in total nine simulation configurations to cover the $St - Ga$ parameter space, which are summarised in Tables 2 and 3, and Figure 2. Notice that the corresponding values of Ga^2 are also listed in the tables, which will be relevant in the discussions on the possible scaling later.

To obtain a representative sample, 10^4 particles were released in the turbulent open channel flow. Note that this number of particles is set arbitrarily and simply to capture the qualitative distributions, rather than to predict the realistic concentration values. Consequently, the particle volume fraction resulting from the above specific number of particles is far higher than the actual value of the microplastic in nature and, therefore, irrelevant. Each simulation was started from a random distribution, which is then evolved and converged to statistically steady distributions. Upon distributing particles, we constrained their locations in a way that they cannot be placed within $2d_p$ from the nearest no-slip/free-slip boundaries to avoid overlapping.

TABLE 2 Particle simulation parameters for the open channel flow at Re_τ = 180.

Case	St	Ga (Ga^2)	d_p^+	$d_{p,real}$ (μm)	$\Delta T_p u_\tau^2/\nu$	$\Delta T_p u_b/h$
A	0.05	0.316 (0.1)	0.97	11.3	3962	346
B		1.0 (1.0)			9755	851
C		3.16 (10.0)			3962	346
D	0.5	0.316 (0.1)	3.08	36	3962	346
E		1.0 (1.0)			3962	346
F		3.16 (10.0)			3399	296
G	5.0	0.316 (0.1)	9.73	113	3962	346
H		1.0 (1.0)			3962	346
I		3.16 (10.0)			3962	346

Note: The $d_{p,real}$ values refer to a natural river.

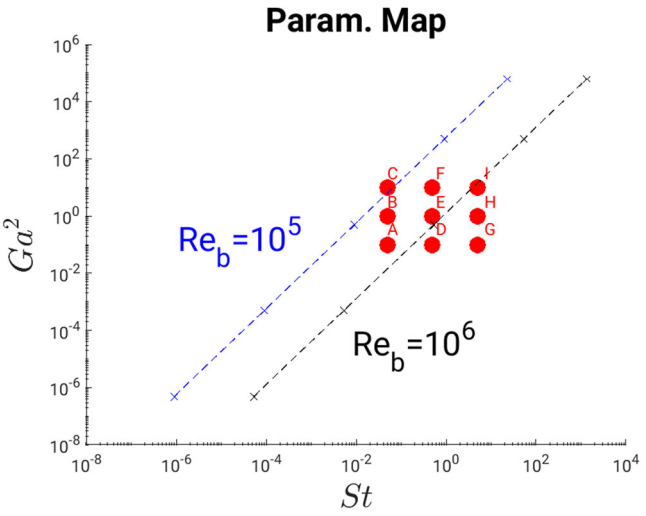

FIGURE 2 Parameters of the simulated dimensionless particle properties. The dashed lines correspond to particles with β = 0.95 and different diameters in one laboratory flume (Re_b= 10^5) and a natural flow (Re_b= 10^6).

At Re_τ = 180, the instantaneous locations and the velocities were sampled every 50 flow timesteps, whereas 750 flow timesteps interval was chosen for Re_τ = 400 due to much finer temporal resolution for the higher Reynolds number case. Subsequently, the extent of the transient periods was determined in terms of the particle concentrations in the near-wall "buffer layer" ($z^+ < 30$), the "free surface" ($z/h > 0.85$) and the rest of the channel namely the "bulk" regions. In each region, the transient period is considered to be over when the deviation of the instantaneous concentration from the final moving-average value, based on the 51 sampling points at the end, goes under 1% after normalisation with the average itself.

Once the above criterion was met, the steady-state concentration profiles were sampled over the period ΔT_p, which can be found in Table 2.

SINGLE-PHASE FLOW VALIDATION

Before proceeding to the particulate flow results, we validate the flow solver in terms of single-phase turbulent statistics of the open channel flow at Re_τ = 180 and 400. Our reference DNS data is from the closed channel flow of the same Reynolds numbers, which was published in Moser et al. [43].

Due to the statistical symmetry of this closed channel configuration, we compare the results from the bottom no-slip wall to the channel semiheight, to the entire depth of the corresponding open channel results. Correspondingly, the reference length-scale for nomalisation h in the closed channel is the channel semiheight. We expect that the turbulent statistics near the bottom no-slip walls are practically identical, whereas they should differ significantly near the free surface. This is because the free-slip boundary condition in the open channel configuration imposes impermeability not only statistically but also instantaneously, whereas the statistical symmetry in the closed channel flow does not—therefore, fluid elements are free to travel across the closed channel semi height instantaneously.

Figure 3 shows the mean streamwise velocity normalised in wall units. Note that the operator $\langle\cdot\rangle$ implies that the ensemble average in time and in space in the two homogeneous directions was applied. Our simulation results and the reference data are almost indistinguishable in both Reynolds number cases.

Figure 4 depicts the root-mean-square of turbulent velocity fluctuations around the mean, that is,

$$u_i' = u_i - \langle u_i \rangle. \tag{12}$$

As expected, the profiles of the turbulent fluctuations match very well with the reference data near the no-slip wall, whereas there exist noticeable deviations near free surface/channel semiheight. In the case of open channel flow where the impermeable free-slip boundary is placed, the turbulent fluctuations in the plane-normal direction ($u_3' = w'$) are dampened progressively towards the free surface, and the corresponding kinetic energy is re-distributed into the orthogonal directions. Moreover, through the energy redistribution the spanwise component receives more energy than the streamwise counterpart, which is well-known phenomenon in open channel turbulence (see e.g., [30, 31, 33]).

RESULTS

In this section, we document the results of microplastics in turbulent open channel flow simulations with different Galileo and Stokes numbers. We consider two different Reynolds numbers, namely Re_τ= 180 and 400. Such flow configurations can be interpreted as idealised configurations of a natural river or a laboratory channel. Whilst all the particle simulation cases (A–I) were performed at Re_τ = 180, only cases A, C, F and G were simulated at Re_τ = 400 due to the significantly more expensive computational cost. Moreover, for the same reason, the averaging period of case F is rather short as it will be discussed later.

In the following, we will consider the steady-state concentration distributions first, which is followed by the observations and the discussions on the emerging time scale depending on the governing dimensional parameters, as well as a possible scaling property.

Steady-state concentration and influence of Reynolds number

We start our evaluation with the steady-state particle concentration distribution with St = 5 (case G–I of Table 2), with the Reynolds number at 180. In this largest Stokes number group, the mean particle distributions are largely homogeneous (see Figure 5a, where the particle concentration distributions across the water depth being

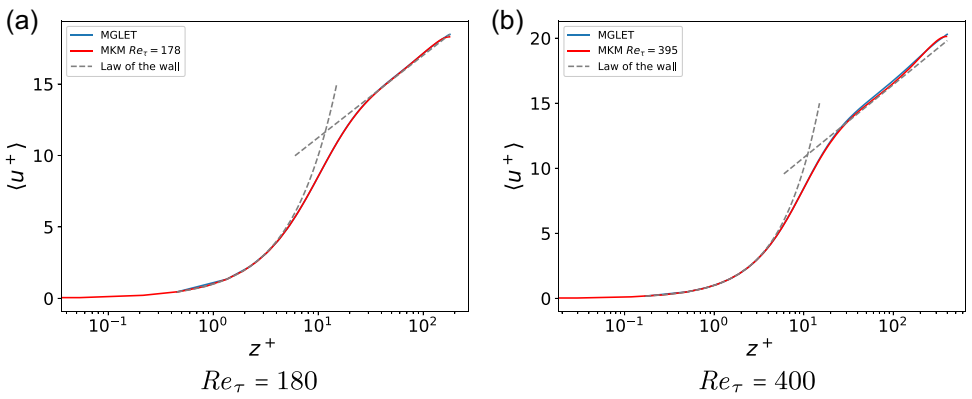

FIGURE 3 Single-phase validation against the direct numerical simulation data set of [43] denoted as MKM. Mean streamwise velocity normalised by u_τ as a function of z^+. Dashed lines represent the logarithmic law of the wall $\langle u^+ \rangle = \frac{1}{\kappa} \ln z^+ + B$, where (a) κ = 0.4 and B = 5.5; (b) κ = 0.41 and B = 5.2. (a) Re_τ= 180, (b) Re_τ= 400.

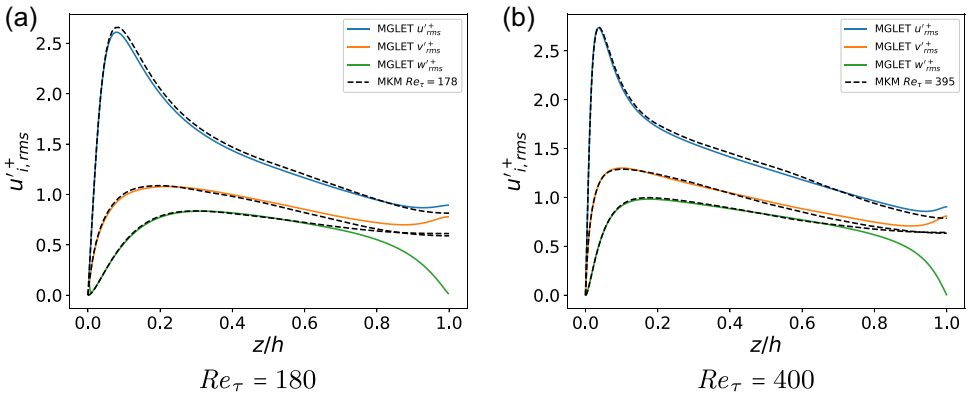

FIGURE 4 Single-phase validation against the DNS data set of [43] denoted as MKM. Root-mean-square of turbulent velocity fluctuations $u'_{i,rms}$ normalised by u_τ as a function of z/h (a) Re_τ= 180, (b) Re_τ= 400.

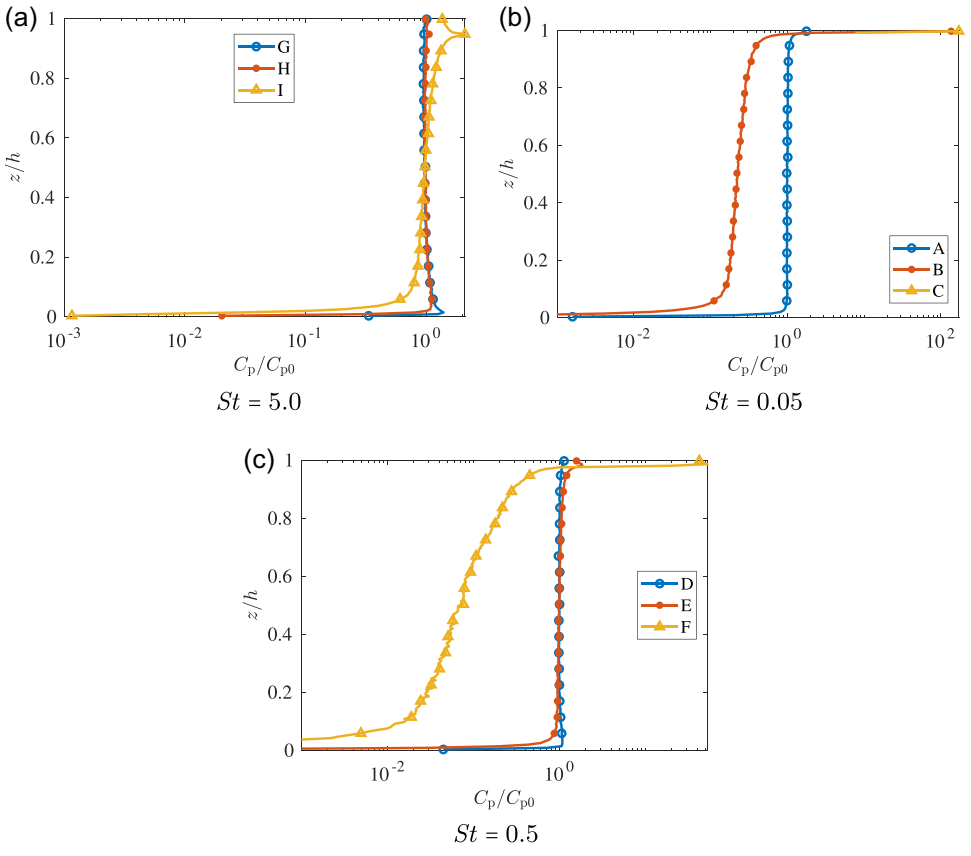

FIGURE 5 Mean particle concentration distribution over the flow depth $C_p(z)$, normalised by the bulk concentration C_{p0}. The line colour and markers distinguish the different cases (a) St = 5.0, (b) St = 0.05, (c) St = 0.5.

sampled in the 180 uniformly spaced bins are shown). From a particle dynamics point of view, this large St implies the microplastic particles are under significant influence of inertia that tend to move straight paths (i.e., ballistic movements) independent of the surrounding fluid velocity field, resulting larger particle-fluid velocity difference. At the largest Ga (case I), a slight accumulation of particles is visible at the surface, and a minor but visible Galileo number effect was observed near the bottom wall, where the thickness of the near-wall nonuniform concentration layer slightly increases with increasing Ga (i.e., stronger buoyancy effect).

Also, in the near-wall region, so-called *turbophoresis* can be observed for the smallest Ga (case G). Turbophoresis refers to the migration and the preferential concentration of light inertial particles towards the regions of lower turbulent diffusivity [44]. This

phenomenon has been studied mostly in the presence of no-slip walls (e.g., [45, 46]), however, it can also be observed near free surface [47], or even without any boundaries [44].

If we reduce the Stokes number significantly, the buoyancy has a much stronger influence on the mean concentration distribution. Figure 5b shows how the concentration at $St = 0.05$ varies depending on the Galileo number (cases A–C). Whilst particles with $Ga = 0.316$ (case A) are almost evenly distributed over the water column, they accumulate completely on the free surface at $Ga = 3.16$ (case C). At $Ga = 1.0$ (case B), a large majority of the particles (≈80% of the total number within the top 10% of the water column) are in the free surface region, whilst the rest of the particles are distributed across the water column, manifesting as an intermediate state between the total accumulation and the uniform distribution. Once again, the thickness of "concentration boundary layer" at the bottom wall grows with increasing Galileo number.

In Figure 5c, the mean concentration distributions at the intermediate Stokes number $St = 0.5$ are shown. The particles are almost uniformly distributed at $Ga = 0.316$ (case D), whilst at $Ga = 1.0$ (case E), a slight accumulation can be observed. On the other hand, a vast majority (≈95% in the top 10% of the water depth) of the particles are clustered near the free surface at $Ga = 3.16$ (case F).

These simulation results show that the Stokes and Galileo numbers do indeed have a large influence on the particle distribution in turbulent free-surface flows. The particles could either completely rise to the free surface (case C), evenly distributed in the water column (case A, D, E, G, H, I), or somewhere in between (case B, F). Which distribution state emerges depends on two competing physical processes: The buoyancy which tries to bring the particle towards the free surface and let them accumulate, and the turbulent fluctuations which helps to redistribute the particles throughout the water column. Our simulations show that the degree of the free-surface accumulation increases with increasing Galileo number if the Stokes number is kept at a constant, which was to be expected. If the Galileo number is kept constant instead, on the other hand, the accumulation intensifies with decreasing Stokes number. At first glance, this is counter-intuitive as with a smaller Stokes number, the particles can adjust more quickly to the fluid velocity, which could result in better vertical mixing. On the other hand, an increase of the Stokes number leads to a decrease of the particle's rising velocity u_t (see Equation 11), which competes with the turbulent velocity fluctuations in the vertical direction to determine whether a particle fraction can accumulate at the free surface.

Under a given gravity condition, the Galileo number is solely determined by the particle characteristics, that is, by a specific $d_p - \beta$ combination. Conversely, the Stokes number—the ratio of particle to flow time scales—is influenced by the flow condition in addition to the particle characteristics. Recall that the flow condition is controlled by the Reynolds number. Consequently, an identical particle has a Stokes number smaller by more than one order of magnitude in a laboratory flume, for example, than in a large natural river (see Figure 2). Therefore the concentration distributions that are determined in the laboratory flume cannot be directly compared to the natural environment.

Next, we examine to what extent the particle distributions are affected by the difference in the Reynolds number, with respect to the $Ga - St$ combinations that were used earlier. This part of the investigation corresponds to, for example, performing experiments in two different laboratory flumes (with different Reynolds numbers), in which the diameter and density ratios of the particles are adjusted to match the dimensionless numbers between the two experiments. This investigation, therefore, approaches the question whether the particle distributions are an exclusive function of the particle-related dimensionless numbers (i.e., Ga and St), or the flow Reynolds number influences the distribution as well.

As mentioned at the beginning of this section, due to the increased numerical effort required for the higher Reynolds number simulations, we selected cases A ($St = 0.05$, $Ga = 0.316$), C ($St = 0.05$, $Ga = 3.16$), F ($St = 0.5$, $Ga = 3.16$) and G ($St = 5.0$, $Ga = 0.316$) to be computed until the steady state. Cases A and G exhibit uniform distributions at $Re_\tau = 180$ over the water column, whilst case F leads to an accumulation of the particles on the free surface. Additionally, we choose case G, since the distribution of this case is very sensitive to the terms being considered in the Maxey–Riley equation. More specifically, we observed that this case experiences an exaggerated turbophoresis if fluid acceleration term is neglected. Note that this observation was also true in case H and I (not shown).

Figure 6 compares the concentration distributions between the two Reynolds numbers. Generally speaking, there is visible but relatively minor Reynolds number dependence in the particle distributions. The biggest effect appears in case F, in which the accumulation at the free surface appears to be equally strong. However, the stronger turbulent mixing, which is the consequence of higher Re_τ, leads to a more even particle distribution in the remaining of water column. The transition layer at the bottom-wall appears to be somewhat thinner for the higher Reynolds number. This comparison leads to the conclusion that, to the limit of the current Reynolds number range, the Reynolds number has no visible qualitative influence on the particle distribution and quantitatively exerts little influence.

In the following, we attempt to explain the above relatively small influence of Re_τ to the vertical particle concentration distributions. Recall that the type of particle concentration distribution is a consequence of the competition between buoyancy, which forces the particles to accumulate toward the free surface, and the turbulent velocity fluctuations in the vertical direction which act to redistribute the particles. This implies that the balance between the terminal rise velocity u_t and the vertical component of the turbulent normal stress w'_{rms} should play a critical role. Furthermore, in closed channel flow, it is known that w'_{rms} scales with u_τ throughout the flow domain except the close proximity of the walls [48], and the same trend can be observed in our open channel data (see Figure 4). Therefore the following relation should be valid except near the boundaries:

$$\frac{u_t}{w'^{+}_{rms}} \sim \frac{u_t}{u_\tau}. \tag{13}$$

Now, recall the definitions of u_t, St and Ga, then:

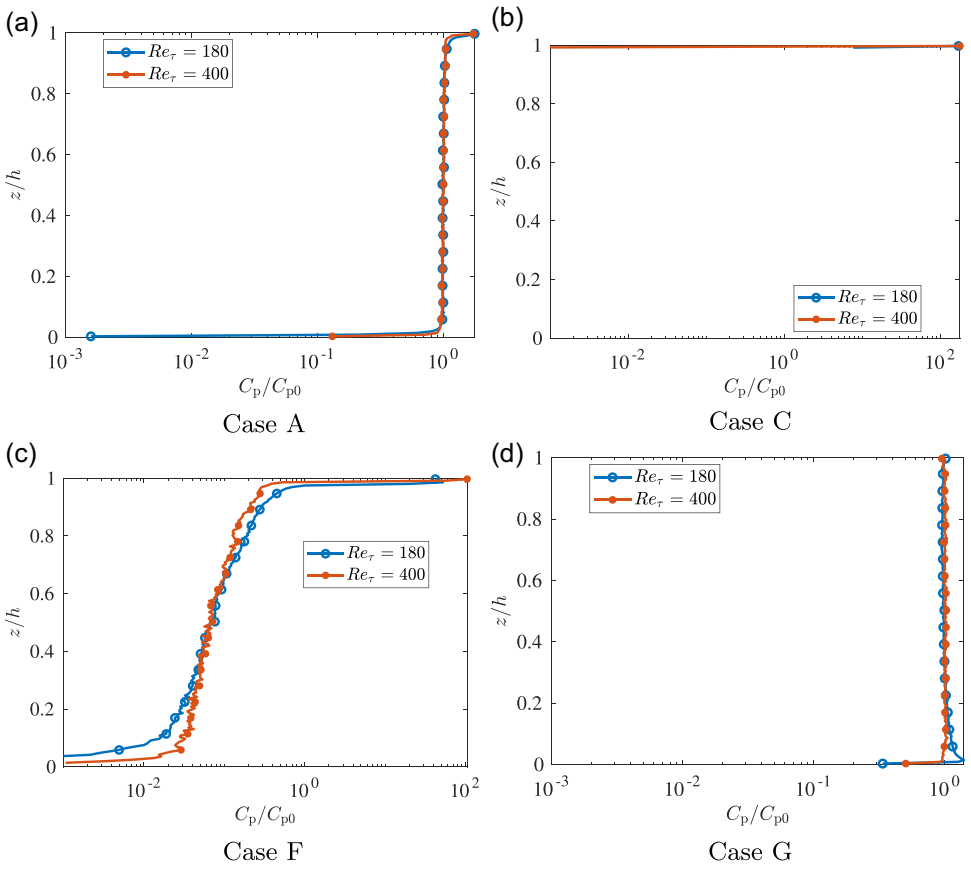

FIGURE 6 Mean particle concentration over the flow depth $C_p(z)$, normalised by the bulk concentration C_{p0}. The line colour and markers distinguish the different Re_τ (a) Case A, (b) Case C, (c) Case F, (d) Case G.

$$\frac{u_t}{u_\tau} = \frac{Ga^2\sqrt{\frac{\beta}{18}}}{\sqrt{St}}. \tag{14}$$

Therefore, the above scaling relation yields a consistent result to our observation that change in Re_τ does not qualitatively influence the particle distribution type for given St and Ga, at least in the bulk flow region.

Moreover, when the above velocity ratio is larger more likely it is that the particles accumulate towards the free surface. It is consistent with the observed trend for the Re_τ= 180 flow that increasing Ga and decreasing St contribute favourably to the free-surface particle accumulation.

Temporal evolution

Next, we investigate the transient behaviour of microplastic concentration distributions. As mentioned in Section 3, the particles are initially randomly distributed in the computational domain. The particles are then redistributed by the turbulent flow, and the distribution eventually reaches a certain statistically steady profile depending on the simulation parameters. In the following, we focus on what happens in the transient phase and in particular, how long it takes from the initial random distribution to the statistically steady state. Note that this question is not only theoretically significant but also needs to be answered from a practical point of view as follows.

Suppose the performance of different sampling strategies of microplastic particles are to be evaluated experimentally in a laboratory flume. For the measured performance to be relevant to the real-world condition, it is crucial that the particle distribution reaches to the statistically steady profile in before the sampling. The question here is whether the experimental setup is long enough to achieve a statistically steady particle distribution. Answering the aforementioned question, therefore, enables us estimate how far downstream from the inlet (or the particle releasing location) the footprint of the initial nonphysical concentration distribution is expected to remain. Note that with our simulations, we can determine the time until a statistically steady-state is reached. This time can then be converted into a distance travelled using the mean flow velocity.

In the following, we first consider the qualitative behaviour, which is followed by a discussion on the topic of possible scaling. Finally, we conclude by discussing possible underlying physical mechanisms. The last step should allow us to check the validity of our results for flow conditions that are not in our parameter space.

Figure 7 illustrates the development from the initial random particle distribution to the equilibrium state. As a measure, we consider the concentration of particles in the top layer, which is

defined as the upper 15% of the water column, as a function of time ($C_{p,top}(t)$). Recall that to avoid potential overlap between the particles and the bottom wall and the free surface, the particles cannot be spawned within the two particles diameter from the nearest boundaries. This restriction results a slight discrepancy among the cases at $t = 0$. Figure 7a,b show different $Ga-St$ combinations at $Re_\tau = 180$, whereas Figure 7c compares case F from $Re_\tau = 180$ and $Re_\tau = 400$. This case F was chosen due to its longest transient time among the simulated $Re_\tau = 400$ cases.

In Figure 7a, the time is expressed in viscous units, that is, $t^+ = tu_\tau^2/\nu$. Notice that the normalisation factor is the time constant which is used to calculate the Stokes number. Conversely, in Figure 7b,c, the normalised times are further multiplied by the governing dimensionless numbers Ga, Re_τ and d_p^+.

In Figure 7a, the concentration in the top layer increases significantly only in cases B, C and F, where there is a significant accumulation of the floating particles. For the smallest particles ($St = 0.05$), the statistically steady state is reached much faster when the Galileo number is larger. Case C ($St = 0.05$, $Ga = 3.16$), for example, reaches its statistically steady distribution after approximately 800 viscous units, whilst case B ($St = 0.05$, $Ga = 1$) needs approximately 8000 viscous units. The ratio of the transient time τ between cases C and B is thus about $\tau_C/\tau_B = 1/10$. Notice that this ratio coincides with the ratio of the two corresponding Galileo numbers squared (Ga^2, see Tables 2 and 3).

A possible explanation to this scaling behaviour of the transient time with respect to Ga, and possible dependence to the flow Reynolds number, can be obtained from the definition of the Galileo number. Recall that Ga^2 is defined as the particle Reynolds number based on the particle rising velocity due to buoyancy u_t (see Section Governing parameters). Then the transient time (t_{rise}) can be seen as the time required for a particle to find an equilibrium vertical position in the channel. The average travelling distance of such particle before finding the equilibrium position should be proportional to the channel height h, whilst the particle position converges to the equilibrium at a rate that is proportional to u_t. Therefore the transient time can be approximated as:

$$t_{rise} \approx \frac{h}{u_t}. \tag{15}$$

If we normalise this estimated transient time by the viscous wall unit of the flow, and using the fact that $u_t = Ga^2\frac{\nu}{d_p}$, then:

$$t_{rise}^+ = \frac{h}{u_t}\left(\frac{u_\tau^2}{\nu}\right) = \frac{hd_p}{Ga^2\nu}\left(\frac{u_\tau^2}{\nu}\right) = d_p^+\frac{Re_\tau}{Ga^2}. \tag{16}$$

Alternatively:

$$t_{rise}^+ = \frac{d_p}{h}\left(\frac{Re_\tau}{Ga}\right)^2. \tag{17}$$

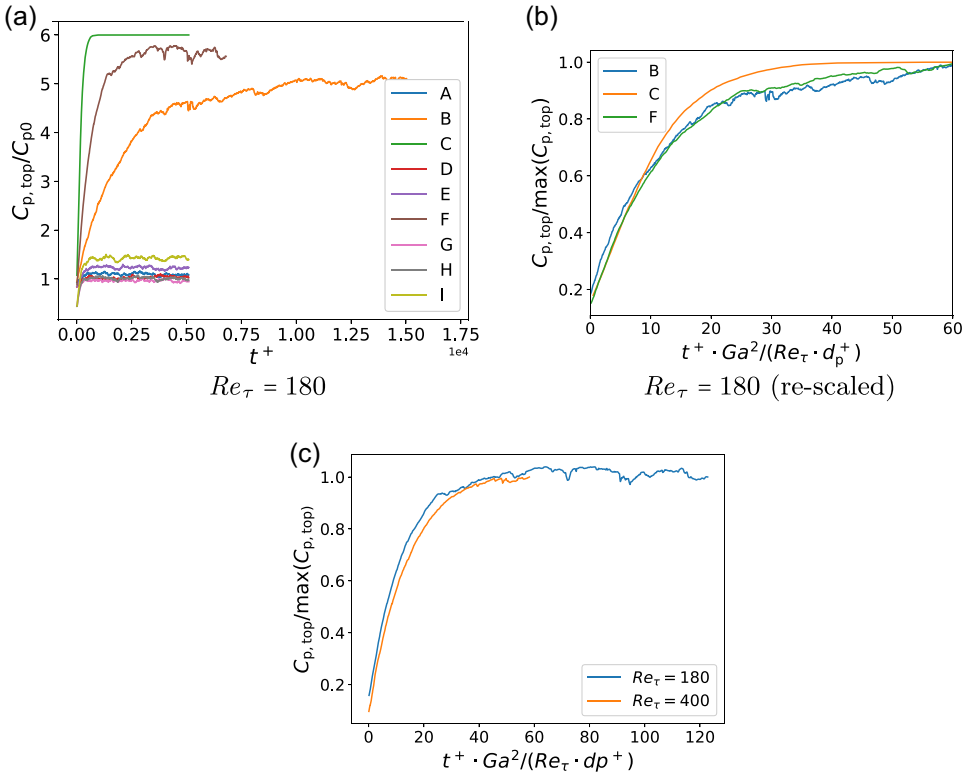

FIGURE 7 Evolution of concentration in the top 15% of channels. The plotting time interval in (b) is limited for better visibility (a) $Re_\tau = 180$, (b) $Re_\tau = 180$ (rescaled), (c) $Re_\tau = 180$ and 400 (case F, rescaled).

TABLE 3 Particle simulation parameters for the open channel flow at Re_τ = 400.

CASE	*St*	*Ga* (Ga^2)	d_p^+	$d_{p,real}$ [μm]	$\Delta T_p u_\tau^2/\nu$	$\Delta T_p u_b/h$
A	0.05	0.316 (0.1)	0.97	11.3	8072	352
C		3.16 (10.0)			6016	262
F	0.5	3.16 (10.0)	3.08	36	2534	110
G	5.0	0.316 (0.1)	9.73	113	3105	135

Note: The $d_{p,real}$ values refer to a natural river.

Notice that both expressions predict Ga^{-2}-scaling of the transient time, which was observed in Figure 7a.

Consequently, the above transient time scaling was applied in Figure 7b. Here we test the validity of the above scaling hypothesis with respect to d_p^+ and *Ga*, whilst Re_τ remains unchanged. Note that for the sake of visibility, the *y*-axis of the plot was also rescaled by the individual maximum concentration levels. Notice that the curves corresponding to case B and F—the two cases belonging to the intermediate concentration distribution group—collapse very well. Moreover, the curve from the case C, which exhibits a complete particle accumulation on the free surface, also follows a similar trajectory. Note that the curves from all other cases are omitted since they do not experience any major transformation of the particle concentration distributions from their initial conditions, therefore, this scaling of time does not apply.

Subsequently, Figure 7c compares the transient behaviour of the particles with *St* = 0.5 and *Ga* = 3.16 (Case F) for the two Reynolds numbers 180 and 400. The good agreement between the two curves supports the validity of our scaling hypothesis with respect to Re_τ.

To this end, it is important to mention that the actual particle sinking/rising velocities within a turbulent flow are strongly influenced by the interactions between the particles and the highly fluctuating flow structures. Therefore the a priori estimation of such velocities is not an obvious task. We have seen from the final concentration profiles that not all nominally buoyant particles actually accumulate at the free surface. The present results indicate that, at least in the situations in which the particles accumulate on the free surface, our simple estimation clearly reflects the magnitude of the time it takes for the particles to rise. However, more simulations should be carried out—also with higher Reynolds numbers—to be able to make definitive statements.

CONCLUSION

Our investigations have revealed the following results on the distribution of weakly buoyant microplastic particles in turbulent open channel flow as an idealisation of natural river. The dynamics of spherical microplastic particles is determined by the following four dimensionless numbers: the flow Reynolds number, the dimensionless particle diameter, the Stokes number and the Galileo number of the particles. A microplastic particle goes through a diverse range in the parameter space, depending on aging, growth in size by biofilm development on the surface, and change in the water body characteristics (e.g., temperature) in which the particle is located. It is therefore required for the investigation to cover a sufficient range to grasp an overall picture of the microplastic dynamics in nature. Consequently, we have selected nine different configurations in terms of the Stokes–Galileo parameter plane, whereas we simulated two different flow Reynolds numbers.

The simulation results show that the steady-state distributions are indeed functions of the Stokes and Galileo numbers. Generally, for large Galileo numbers, the particles accumulate at the free surface, whereas for small Galileo numbers, they remain homogeneously distributed over the water column. The critical Galileo number limit where the distribution pattern changes qualitatively depend on the Stokes number, which makes it very difficult to be precisely determined.

The particle dynamics also depend on the flow Reynolds number. Despite the fact that we could only achieve a relatively low Reynolds number range, the corresponding dependency is noticeable.

When the particles float to the free surface, they do so, at least in these considered cases, with a time constant resulting from the rate of ascent in a quiescent fluid. Finally, a result that can be seen surprising is that not all particles that are lighter than the surrounding fluid float, as the turbulent flow can move the particles up and down much faster than gravity.

ACKNOWLEDGEMENTS

The financial support provided by the German Federal Ministry of Education and Research (BMBF) (grant number: 02WPL 1442G) is greatly acknowledged by the authors. Computing time was provided by Leibniz Supercomputing Center of the Bavarian Academy of Sciences and Humanities. YS thanks his former and current students, Mr T. Wieder and Mr F. Schaefer, for their contributions as a thesis student and a research assistant, respectively. Finally, the authors thank the anonymous reviewers for their careful reading of our manuscript and their many insightful criticisms and suggestions.

CONFLICT OF INTEREST STATEMENT

The authors declare no conflict of interest.

DATA AVAILABILITY STATEMENT

Research data are not shared.

ORCID

Yoshiyuki Sakai http://orcid.org/0000-0001-8125-6566

REFERENCES

[1] N. B. Hartmann, T. Hüffer, R. C. Thompson, M. Hassellöv, A. Verschoor, A. E. Daugaard, S. Rist, T. Karlsson, N. Brennholt, M. Cole, M. P. Herrling, M. C. Hess, N. P. Ivleva, A. L. Lusher, M. Wagner, *Environ. Sci. Technol.* **2019**, *53*(3), 1039.

[2] J. R. Jambeck, R. Geyer, C. Wilcox, T. R. Siegler, M. Perryman, A. Andrady, R. Narayan, K. L. Law, *Science* **2015**, *347*, 768.
[3] L. Hildebrandt, N. Voigt, T. Zimmermann, A. Reese, D. Pröfrock, *Marine Environ. Res.* **2019**, *151*, 104768.
[4] S. Keßler, T. Pohlert, V. Breitung, K. Wilcsek, R. Bierl, *Environ. Sci. Pollut. Res.* **2020**, *27*, 5993.
[5] L. Mai, L. -J. Bao, L. Shi, C. S. Wong, E. Y. Zeng, *Environ. Sci. Pollut. Res.* **2018**, *25*, 11319.
[6] L. Hildebrandt, T. Zimmermann, S. Primpke, D. Fischer, G. Gerdts, D. Pröfrock, *J. Hazard Mater.* **2021**, *414*, 125482.
[7] C. G. Bannick, U. Braun, D. Herper, A. Kerndorff, M. Knefel, M. Ricking, L. Zechmeister, K. Altmann, Probenahmemethodik zur Messung von Mikroplastik: Wie erhält man eine repräsentative Probe? Technical report, Factsheet 10.3 des BMBF-Forschungsschwerpunkts Plastik in der Umwelt, **2021**.
[8] T. Mani, A. Hauk, U. Walter, P. Burkhardt-Holm, *Sci. Rep.* **2015**, *5*, 17988.
[9] J. G. M. Kuerten, *Flow Turbul. Combust.* **2016**, *97*(3), 689. https://doi.org/10.1007/s10494-016-9765-y
[10] M. R. Maxey, *Phys. Fluids* **1983**, *26*(4), 883. https://doi.org/10.1063/1.864230
[11] S. Lovecchio, C. Marchioli, A. Soldati, *Phys. Rev. E Stat. Nonlin. Soft Matter Phys.* **2013**, *88*(3), 2. https://doi.org/10.1103/PhysRevE.88.033003
[12] H. Rouse, in *Exhib. D Rep. Comm. Sedimentation*, National Research Council, Washington, D.C. **1938**, pp. 57-64. https://resolver.caltech.edu/CaltechAUTHORS:20140602-155323565
[13] M. Manhart, *Comput. Fluids* **2004**, *33*(3), 435. https://doi.org/10.1016/S0045-7930(03)00061-6
[14] N. Peller, A. LeDuc, F. Tremblay, M. Manhart, *Int. J. Num. Methods Fluids* **2006**, *52*(11), 1175. https://doi.org/10.1002/fld.1227
[15] J. H. Williamson, *J. Comput. Phys.* **1980**, *35*(1), 48. https://doi.org/10.1016/0021-9991(80)90033-9
[16] A. J. Chorin, *Math. Comput.* **1968**, *42*(3), 490. http://www.ams.org/journals/mcom/1968-22-104/S0025-5718-1968-0242392-2/S0025-5718-1968-0242392-2.pdf
[17] N. Peller, *PhD Thesis*, Technische Universität München **2010**.
[18] Y. Sakai, M. Manhart, *Flow, Turbul. Combust.* **2020**, *105*, 581. https://doi.org/10.1007/s10494-020-00168-4; http://link.springer.com/
[19] Y. Sakai, S. Mendez, H. Strandenes, M. Ohlerich, I. Pasichnyk, M. Allalen, M. Manhart, in *Proc. Platf. Adv. Sci. Comput. Conf. PASC '19*, Vol. 78000, ACM Press, New York, New York, USA **2019**, pp. 1-13. https://doi.org/10.1145/3324989.3325716
[20] S. Elghobashi, *Appl. Sci. Res.* **1991**, *48*(3-4), 301. https://doi.org/10.1007/BF02008202
[21] R. Clift, J. R. Grace, M. E. Weber, *Bubbles, Drops, and Particles*, Dover, Mineola, NY **2005**.
[22] D. E. Faleiros, M. Tuinstra, A. Sciacchitano, F. Scarano, *Exp. Fluids* **2021**, *62*(9), 1. https://doi.org/10.1007/s00348-021-03274-9
[23] K. Guseva, A. Daitche, U. Feudel, T. Tél, *Phys. Rev. Fluids* **2016**, *1*(7), 1. https://doi.org/10.1103/PhysRevFluids.1.074203
[24] S. Olivieri, F. Picano, G. Sardina, D. Iudicone, L. Brandt, *Phys. Fluids* **2014**, *26*(4), 00. https://doi.org/10.1063/1.4871480
[25] S. Tajfirooz, J. G. Meijer, R. A. Dellaert, A. M. Meulenbroek, J. C. H. Zeegers, J. G. M. Kuerten, *J. Fluid Mech.* **2021**, *910*, 1. https://doi.org/10.1017/jfm.2020.1001
[26] M. A. T. van Hinsberg, J. H. M. tenThijeBoonkkamp, H. J. H. Clercx, *J. Comput. Phys.* **2011**, *230*(4), 1465. https://doi.org/10.1016/j.jcp.2010.11.014
[27] M. A. T. Van Hinsberg, H. J. H. Clercx, F. Toschi, *Phys. Rev. E* **2017**, *95*(2), 023106. https://doi.org/10.1103/PhysRevE.95.023106
[28] C. Gobert, M. Manhart, *J. Comput. Phys.* **2011**, *230*(21), 7796. https://doi.org/10.1016/j.jcp.2011.06.028
[29] V. Borue, S. A. Orszag, I. Staroselsky, *J. Fluid Mech.* **1995**, *286*, 1.
[30] R. A. Handler, T. F. Swean Jr., R. I. Leighton, J. D. Swearingen, *AIAA J.* **1993**, *31*(11), 1998. https://doi.org/10.2514/3.11883
[31] S. Komori, R. Nagaosa, Y. Murakami, S. Chiba, K. Ishii, K. Kuwahara, *Phys. Fluids A Fluid Dyn.* **1993**, *5*(1), 115. https://doi.org/10.1063/1.858797
[32] K. Lam, S. Banerjee, *Phys. Fluids A Fluid Dyn.* **1992**, *4*(2), 306. https://doi.org/10.1063/1.858306
[33] R. Nagaosa, *Phys. Fluids* **1999**, *11*(6), 1581. https://doi.org/10.1063/1.870020
[34] Y. Pan, S. Banerjee, *Phys. Fluids* **1995**, *7*(7), 1649. https://doi.org/10.1063/1.868483
[35] T. F. Swean, R. I. Leighton, R. A. Handler, J. D. Swearingen, AIAA, paper 91-0, **1991**. https://doi.org/10.2514/6.1991-613
[36] G. Wang, D. H. Richter, *J. Fluid Mech. 2019*, *868*, 538. https://doi.org/10.1017/jfm.2019.210
[37] D. K. A. Barnes, F. Galgani, R. C. Thompson, M. Barlaz, Philos. Trans. R. Soc. B Biol. Sci. **2009**, *364*(1526), 1526; https://doi.org/10.1098/rstb.2008.0205
[38] M. Cole, P. Lindeque, C. Halsband, T. S. Galloway, *Mar. Pollut. Bull.* **2011**, *62*(12), 2588. https://doi.org/10.1016/j.marpolbul.2011.09.025
[39] V. Hidalgo-Ruz, L. Gutow, R. C. Thompson, M. Thiel, *Environ. Sci. Technol.* **2012**, *46*(6), 3060. https://doi.org/10.1021/es2031505
[40] C. G. Bannick, R. Szewzyk, M. Ricking, S. Schniegler, N. Obermaier, A. K. Barthel, K. Altmann, P. Eisentraut, U. Braun, *Water Res.* **2019**, *149*, 650. https://doi.org/10.1016/j.watres.2018.10.045
[41] J. Brosda, M. Manhart, *J. Fluid Mech.* **2022**, *932*, A25-1.
[42] F. Schwertfirm, M. Manhart, *Int. J. Heat Fluid Flow* **2007**, *28*(6), 1204.
[43] R. D. Moser, J. Kim, N. N. Mansour, *Phys. Fluids* **1999**, *11*(4), 943. https://doi.org/10.1063/1.869966
[44] F. De Lillo, M. Cencini, S. Musacchio, G. Boffetta, *Phys. Fluids* **2016**, *28*(3), 035104. https://doi.org/10.1063/1.4943274
[45] J. G. M. Kuerten, C. W. M. van der Geld, B. J. Geurts, *Phys. Fluids* **2011**, *23*(12), 123301. https://doi.org/10.1063/1.3663308
[46] C. Marchioli, A. Soldati, *J. Fluid Mech. 2002*, 468, 283. https://doi.org/10.1017/S0022112002001738
[47] C. Narayanan, D. Lakehal, L. Botto, A. Soldati, *Phys. Fluids* **2003**, *15*(3), 763. https://doi.org/10.1063/1.1545473
[48] S. Hoyas, J. Jiménez, *Phys. Fluids* **2006**, *18*(1), 011702. https://doi.org/10.1063/1.2162185

How to cite this article: Y. Sakai, M. Manhart, *Appl. Res.* **2024**;*3*:e202200092. https://doi.org/10.1002/appl.202200092